Arch. Metall. Mater. **70** (2025), 1, 275-284

DOI: https://doi.org/10.24425/amm.2025.152543

V.S.S.H. VARDHAN[1], A. SHARMA[1*]

MECHANICAL PROPERTIES AND TRIBOLOGICAL BEHAVIOR OF GRAIN REFINED WE43 MAGNESIUM ALLOY

In the current work, the surface of WE43 Mg alloy has been modified by friction stir processing (FSP) in order to assess grain refinement on mechanical and tribological properties. After FSP, along with the decreased grain size, the reduced fraction of intermetallics ($Mg_{24}Y_5$, $Mg_{41}Nd_5$) was observed as also confirmed by X-ray diffraction (XRD) analysis. Furthermore, the altered intensity of the significant XRD peaks after FSP indicates the development of texture. Increased micro hardness (from 86.3 ± 7.9 $HV_{0.1}$ to 127.2 ± 3.4 to) and tensile strength (from 207 to 267.2 MPa) at the cost of marginally losing the ductility as reflected in decreased % of elongation from 32.02 to 29.04 were observed in FSPed alloy. The scratch test was conducted by applying three different loads (30 N, 40 N and 50 N) to assess the tribological properties of the FSPed surface. The scratch hardness obtained from the width of the scratch indicated a significant increase in the scratch hardness in the FSPed alloy compared with the base alloy. The results suggest the promising role of modifying surface microstructure by FSP to improve the mechanical performance and tribological characteristics of WE43 alloy.

Keywords: Rare earths; Mg alloys; Mechanical properties; micromechanical testing; FSP; Scratch hardness

1. Introduction

Magnesium (Mg) alloys have become the choice of interest as potential candidates in fabricating light weight structures. Being a light weight material, Mg exhibits relatively lower density and higher specific strength compared with Al [1,2]. Additionally, Mg possesses better damping properties and good castability [3]. However, Mg's lower formability is a limitation due to its hcp crystal structure and poor corrosion resistance. Several alloying elements have been added to the Mg system to produce high performing alloys. Developing special composites [4,5], adopting surface treatments [5], providing surface coatings [5], and tailoring surface topography by machining [6,7] are a few strategies reported in the literature to improve the performance of Mg alloys. On the other hand, microstructural modification is a proven strategy in the processing of materials to enhance their mechanical performance.

The grain refinement along with enhanced bulk properties can be achieved in Mg alloys by using a variety of mechanical processing procedures, such as severe plastic deformation (SPD) or thermomechanical treatments [8,9]. Friction stir processing (FSP), is a solid-state technique that uses a non-consumable tool to plastically stir the surface of the targeted substrate and results in a superior level of grain refinement [10,11]. Since FSP is carried out within the solid state, the complexity of handling liquid Mg can be completely eliminated. Particularly, for highly reactive metals such as Mg, FSP is a promising technique to bring fine grain structure without melting the workpiece 12]. Pure Mg [13] and several Mg alloys including AZ31 [14], AZ61 [15], AZ91 [16], AZ80 [17], ZE41 [18], ZK60 [19], AM60, and Mg-RE (Y, Gd, Nd, Zr) [20-22] have been processed by FSP and significant grain refinement has been achieved.

Rare earth (RE)-containing magnesium alloys have shown improved corrosion and mechanical performance. Aircraft engine components, helicopter rotor heads, racing wheels, motorsport components, engine casings, power transmission and gearbox casings are a few potential applications of RE-containing Mg alloys. The presence of neodymium (Nd) and yttrium (Y) in Mg enhances mechanical and corrosion resistance [23-25]. The addition of Zirconium (Zr) helps to decrease the large columnar grains in Mg. The presence of intermetallics such as $Mg_{41}Nd_5$ and $Mg_{24}Y_5$ due to the added Nd and Y in Mg significantly enhances the mechanical, corrosion and tribological performance of Mg-RE alloys. The quantity, size and distribution of these intermetallics can be altered by heat treatment or mechanical processing that involves recrystallization. From the earlier

[1] VIT-AP UNIVERSITY, SCHOOL OF MECHANICAL ENGINEERING, AMARAVATI, ANDHRA PRADESH, INDIA-522237

* Corresponding author: sharma.ambuj@vitap.ac.in

reports, the fraction and the distribution of intermetallics in Mg alloys can be significantly altered in Mg alloys by FSP [16,19]. Applying 6 passes of FSP increased the alloy's corrosion resistance compared to its original as-annealed condition [26]. This improvement was attributable to the fragmentation and redistribution of second-phase particles. The protective passive layer became more homogeneous after using FSP, and the level of micro-galvanic coupling that causes pitting corrosion was reduced at the same time. Biocompatible WE 43 Mg-based alloys treated using a combination of rotary swaging (RS) and friction stir processing (FSP) concerning different rotational speeds. The evolution of textures and characterizations of grain sizes and grain boundaries were studied [27]. Recently, Wu et al. [28] processed WE43 Mg alloy by FSP at different combinations of tool rotational and travel speeds and a grain refinement was achieved from 27.96 μm to ~4.32 μm. The refined microstructure has a significant effect on enhancing the microhardness and decreasing the intergranular corrosion in phosphate buffer saline solution.

The information on the role of surface grain refinement achieved by FSP on the surface scratch resistance and the mechanical performance of WE43 Mg alloy is insufficient. Hence, in the present work, Mg-Nd-Y-Zr alloy (WE43) has been subjected to FSP with the aim to achieve grain refinement and altering the intermetallics. After that, the role of modified microstructure on mechanical and tribological properties was examined.

2. Materials and methods

WE43 Mg alloy sheets of size 100×100×6 mm^3 were procured from Exclusive Magnesium, India with the chemical composition of 3.5% Y, 2.5% Nd, 0.5% Zr and the remaining being Mg. An FSP tool having a shoulder of 20 mm diameter with a threaded tapered pin of 5 mm length and a radius of 6 to 3 mm has been used to perform the FSP. Fig. 1(a) shows the photograph of the FSP tool used to process the WE43 alloy sheet. The workpiece was fixed on the table of specially designed FSP equipment and the FSP tool was arranged in the spindle and a 1° tilt angle was selected. Usually, the tool tilt angle is adopted during FSP to achieve a higher level of material flow and to apply appropriate hydrostatic pressure by the tool shoulder to avoid excessive material flash from the stir zone. For Mg alloys, lower tool tilt angles are suggested and hence 1° tilt angle was selected in the present work [12,29]. It was reported that the lower tool rotational speeds decrease the heat generation and cause poor material flow and higher tool travel speeds allow insufficient time for stirring of material and results in defects in the nugget zone. Hence, selecting an appropriate combination of process parameters is crucial to achieve a defect free stir zone. In the present work, the process parameters to conduct the FSP experiments were selected based on the literature and presented in TABLE 1 [30,31]. The rotating FSP tool was first placed into the workpiece such that its shoulder was entirely in contact with the workpiece's surface and 30 seconds were given to allow enough heat to build up in the stir zone as a result of the generated friction between the surface of the workpiece and the FSP tool's shoulder. Then the rotating tool was allowed to travel in the traverse direction. Fig. 1(b) depicts a schematic diagram of the procedure, and Fig. 1(c) depicts a picture of the FSPed WE43 alloy. Then the specimens for characterization, mechanical properties evaluation and surface scratch test were prepared by wire electric discharge machining (EDM).

TABLE 1

FSP process parameters adopted to develop grain refined WE43 Mg alloy

Parameter	Value/Characteristics
Tool rotational speed	900 rpm
Tool traverse speed	50 mm/min
Tool tilt angle	1°
Workpiece preheating	No preheating
Tool Material	H16 steel

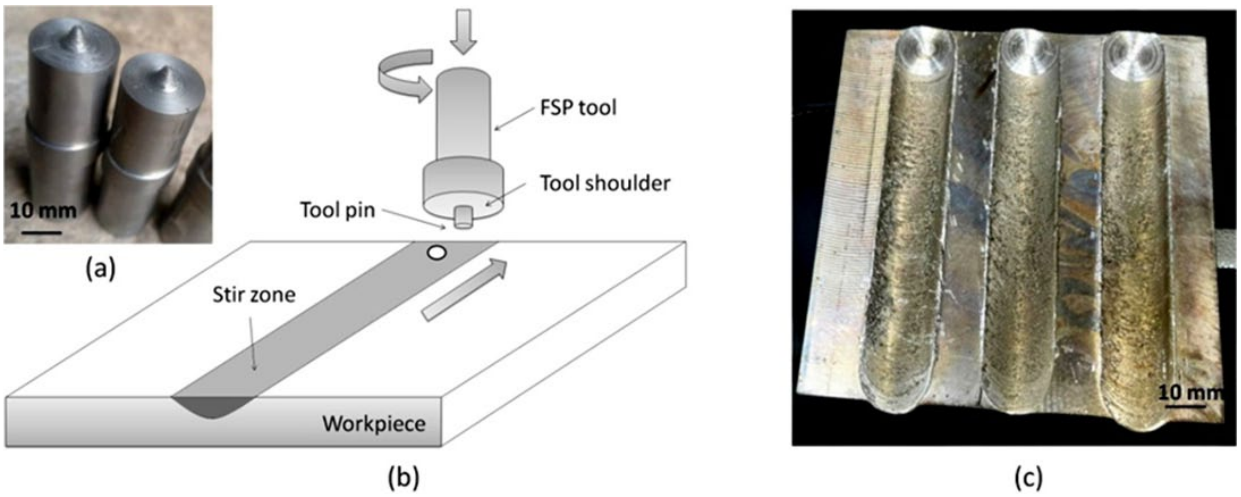

Fig. 1. (a) Schematic representation of FSP process and (b) photograph of FSPed alloy sheet

3. Preparation of specimens for characterizations

3.1. Microstructural analysis

The Metallographic test samples were made based on the ASTM E3-95 method (ASTM E3-95 – 2017). Specimens of the size of (35 × 18 × 10) mm were cut across the FSPed zone and also from the base alloy. The samples were polished in accordance with the normal metallographic method and then etched with a solution of picric acid reagent. An inverted optical microscope (Leica, Germany) and scanning electron microscope (TESCAN, Czech Republic) were used to record the specimens' microstructure. The Stir Zone (SZ) of the FSPed alloy was extracted for XRD, (D8 Bruker, USA) analysis was carried out by using Cu Kα between 20° to 80° 2θ range with a step size of 0.1 and a scan rate of 0.1°/s.

3.2. Mechanical and tribological analysis

To comprehend the impact of microstructural changes on the structural performance of the FSPed alloy, the mechanical characteristics of specimens were assessed. Microhardness measurements were done across the FSP region and compared with the base alloy by using an automated microhardness tester (Omitech, India), by applying a 100 g load (ASTM E92-17 – 2017). Tensile tests were performed by using a 10kN capacity universal testing machine (H10KL/150) to assess the samples' ultimate tensile strength and yield strength. The specimens were prepared as per the ASTM WK49229 (ASTM WK49229 – 2015) standard as shown in Fig. 2 by wire EDM across the FSPed region such that the width of the tensile sample is perpendicular to the FSP direction. Tensile tests were carried out at a strain rate of 0.01 [1/s]. Then the fracture surfaces were examined by using SEM.

A Scratch test was conducted on both the base alloy and FSPed alloy by applying varying loads (20 N and 50 N). Before

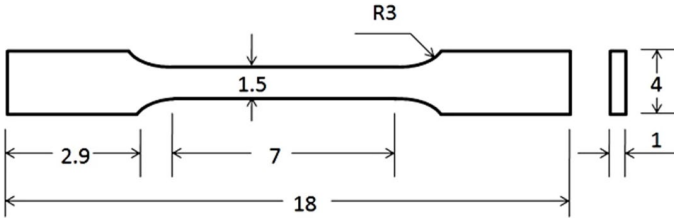

Fig. 2. Dimensions of micromechanical tensile test samples and typical photograph of the samples

the experiments, all the samples were polished up to a common roughness level by using fine grade (2000) emery sheets. Experiments were conducted in dry conditions at room temperature. From the test data, friction coefficient values have been obtained and compared. The average width of the produced scratch has been measured by using ImageJ software (Netherlands) to calculate the scratch hardness by using Eq. (1).

$$H_s = \frac{8P}{\pi\left(\mathrm{D}^2\right)} \tag{1}$$

Where H_s is scratch hardness (MPa), P is applied load (N), and D is the width of the scratch. The width of the scratch has been measured at 10 different regions across the scratch. The mean values have been obtained with standard deviation to compare the scratch hardness. Fig. 3 shows the flow chart of the current research work.

4. Results and discussion

Fig. 4(a) presents the photograph obtained at the cross-section of the FSPed sample that indicates the stir zone free from the tunneling defect. The material flows in the direction

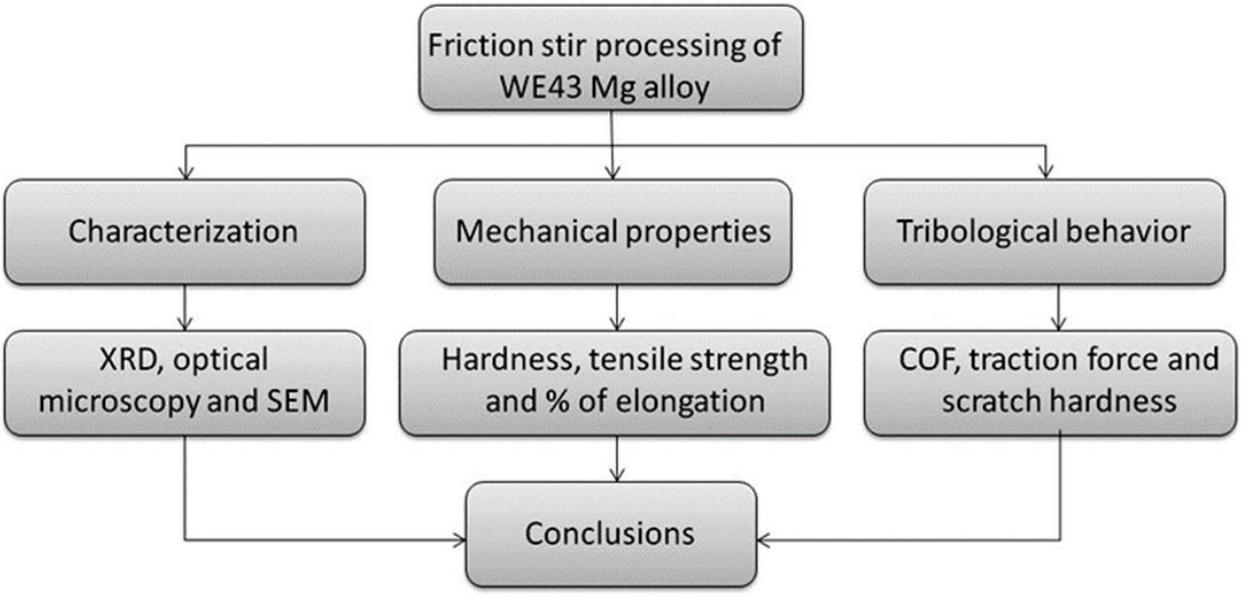

Fig. 3. Flow chart showing the work plan of the current research work

of thickness producing a perfect metallurgical continuity across the processed region. Fig. 4(b) shows the microstructure of the base alloy. From the linear intercept method, the average grain size was measured as 46 ± 4.2 µm. The intermetallics ($Mg_{24}Y_5$, $Mg_{41}Nd_5$) usually appear when Y and Nd are added to Mg and were identified in the base alloy as indicated with arrows at the grain boundaries (Fig. 4(b)). The FSP led to grain refinement that can be observed in the SZ of the FSPed WE43 sample at the cross-section (Fig. 4(b) and 4(c)). The thermomechanical affected zone (TMAZ) and heat affected zone (HAZ), which are next to the SZ, are shown in Fig. 4(c). The SZ (Fig. 4(d)) demonstrates an average grain size of 16.1 ± 5.4 µm. Several twins were also observed in the grains of the stir zone (indicated with arrows in Fig. 4(d)). Due to the HCP crystal structure, Mg exhibits more twins when subjected to plastic deformation. The presence of more twins also influences the material bulk properties as they are also considered crystal imperfections.

The Microstructure of the SZ shows relatively fine intermetallics compared with the base alloy. SEM observations (Fig. 5) also confirm the decreased amount of intermetallic phases and the grain refinement in the FSPed WE43 compared with the base alloy. XRD analysis before and after FSP demonstrates the development of texture (Fig. 6). FSP led to decrease in the peak intensities corresponding to intermetallics ($Mg_{24}Y_5$, $Mg_{41}Nd_5$). This is caused by the heat produced during FSP which increased the solubility limit of the alloying elements and dynamic recrystallization which led to the evolution of new grains with more solubility of alloying elements. Hence, the resulting grains are believed to be supersaturated due to the dissolution of more amount of alloying elements. This is similar to the earlier reported works

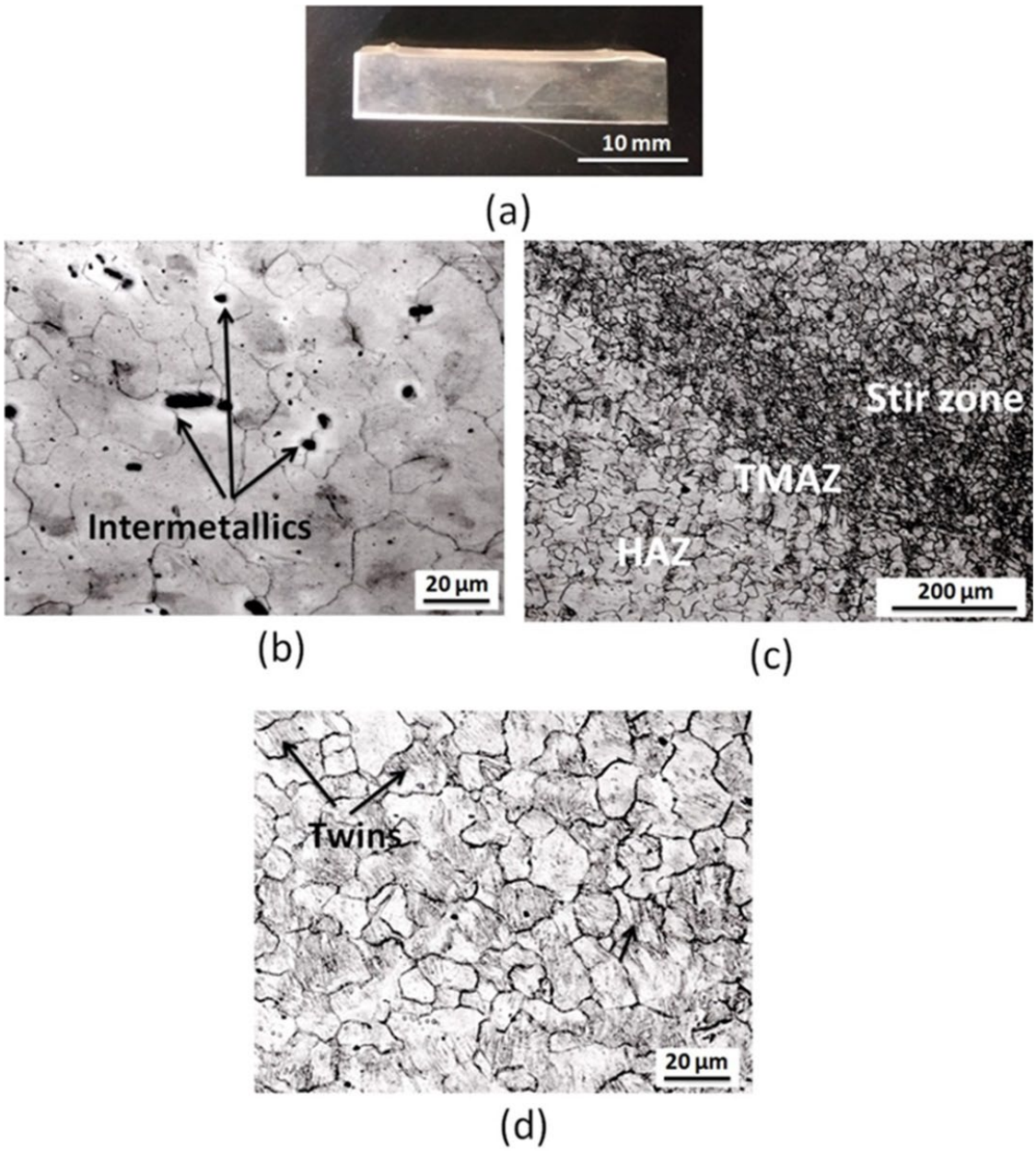

Fig. 4. (a) Photograph of the cross section of FSPed WE43, (b) optical microscope images of WE43 Mg alloy, (c) microstructure in the nugget zone and (d) microstructure at the cross section of FSPed WE43

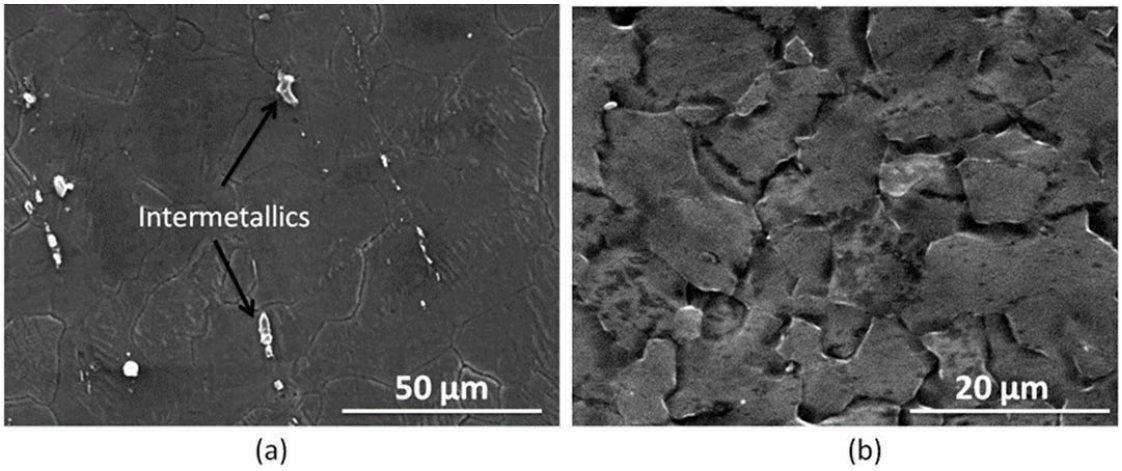

Fig. 5. SEM images of the samples: (a) base alloy and (b) FSPed WE43

in FSP of AZ31, AZ91 and ZE41 Mg alloys where, significant decrease in the fraction of intermetallics and grain refinement are the common observations [16,18,32]. Decreasing the intermetallics and producing smaller grains help to enhance the mechanical performance [32,33]. Furthermore, a significant change in the XRD peak intensities after FSP also suggests the development of texture during the material flow in the SZ of FSPed WE43.

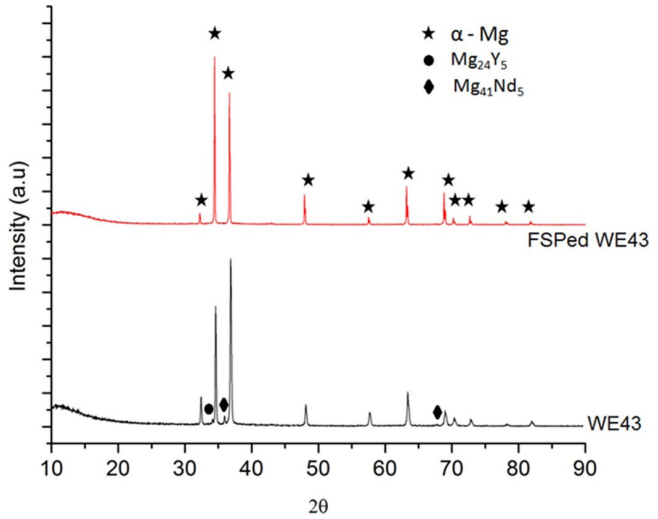

Fig. 6. XRD patterns of the samples

From the microstructures and XRD data of the samples, the following important factors are observed to be influential in altering the bulk properties of the FSPed samples.

(1) Reduced grain size which increases the fraction of grain boundary
(2) Decreased intermetallic quantity.
(3) Supersaturated grains due to the more dissolution of the alloying elements
(4) Texture of the FSPed samples as reflected in the altered peak intensities after FSP.

The above factors certainly affect the structure sensitive properties. For example, grain refinement increases the strength of the FSPed sample. On the other hand, increased grain boundary increases the electrochemical activities at the grain boundaries. Decreased intermetallics reduce the galvanic corrosion in the corroding environment. Supersaturated grains lead to distortion of the lattice and increase the strength of the alloy. Texture in Mg alloys influences the deformation mechanisms under applied mechanical loading. Hence, the combined effect of the aforementioned factors on the mechanical performance of FSPed WE43 is significant.

Fig. 7 presents the microhardness distribution and average values of the samples. It was observed that the SZ has higher hardness compared to that of the base alloy. More variations were noticed in the hardness values for the base material. This kind of observation can be seen in the other Mg alloys including AZ31, ZE41 and AZ91 as reported in the recent literature [14,16,18]. Considering the combined presence of intermetallics and solid solution grains, the change in the distribution of these regions significantly influences the mechanical behaviour as reflected in the uniform hardness values in the present work. A gradual increment in the hardness from the advancing side in the SZ to higher values can also be observed for the FSPed WE43 sample. Increased hardness after FSP is ascertained to the role of microstructure modification in the SZ. Higher hardness was recorded in the centre of the SZ compared with the advancing and retreating sides of the SZ. The presence of smaller grains and also more twins in the SZ compared with TMAZ and HAZ led to an increase in the hardness in the FSPed sample.

Fig. 8 compares the stress-strain plots of the samples before and after FSP. The results indicate improved mechanical properties for the FSPed sample. The ultimate tensile strength was measured as increased to 267.2 MPa compared with the base alloy (207 MPa) after FSP. The ductility was marginally decreased as reflected by the reduced % of elongation from 32.02 to 29.04 after FSP. The increased tensile strength is claimed to the grain boundary strengthening mechanism in the FSPed WE43 sample. Relatively the benefit achieved due to the grain refinement in enhancing the strength is prominent compared with the marginal loss in ductility. It has been well understood in the literature that the supersaturated grains resulted from the decreased intermetallics during FSP enhance the mechanical performance

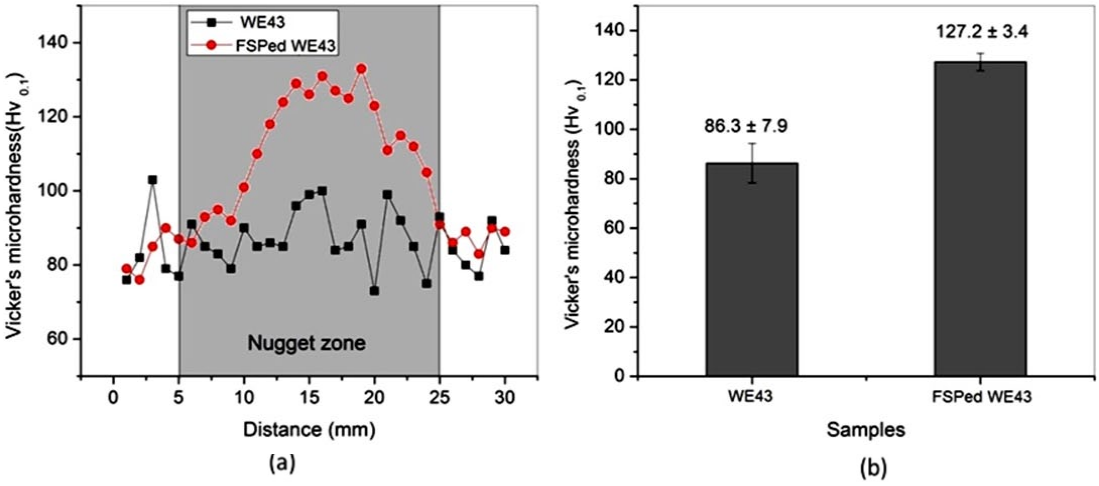

Fig. 7. Microhardness values of the samples: (a) hardness distribution and (b) average hardness values

of Mg alloys [29]. The development of texture after FSP also contributes to improve the tensile strength [29,30]. Furthermore, the stress-strain curves instability was also observed in the plastic region in both the samples. This kind of flow stress instability is influenced by working temperature and strain rate during the plastic deformation of Mg alloys, particularly in the alloys which have intermetallics at the grain boundaries [34,35]. In WE43 Mg alloy, RE containing intermetallics can be observed at the grain boundaries. Even though, FSP decreases the quantity of the intermetallics in Mg alloys, presence of smaller intermetallics is inevitable [16,18,29]. Hence, before fracture, regions with stress instability was observed from the stress-strain curves of both the samples.

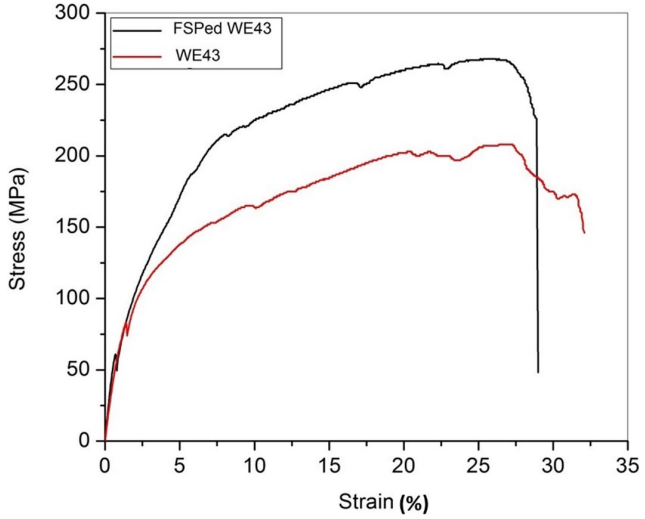

Fig. 8. Engineering stress strain curves of the samples

Fig. 9 presents the morphologies of the fractured surfaces after tensile tests under the applied uniaxial load. More cracks (as represented with circles) resulted due to the removed intermetallics during the failure in the base alloy compared with the FSPed WE43. The corresponding magnified images (Fig. 9(c) and 9(d)) shows the cracks resulted from the fracture as indicated with white arrows. Both the samples exhibited wave patterns of the fractured surface. Due to the decreased intermetallics after FSP, the corresponding cracks were observed as lower in the FSPed WE43.

Fig. 10 presents the photographs of the surfaces of the samples after the scratches test was carried out at three different loads (30, 40 and 50 N). From these images ploughing with a smaller scratch width formation was observed in the FSPed samples. Wear debris was clearly noticed on the base alloy surface adjacent to the produced scratch. On the other hand, lower wear debris was noticed next to the scratch on the FSPed WE43 samples at all loading conditions. As explained by Surya Kiran et al., [24], smaller grains with decreased intermetallics help to produce sound edges without resulting in significant material de-lamination during the material removal process. In the present work, lower debris on the FSPed samples can be claimed to be the refined microstructure due to FSP. Fig. 11 shows the coefficient of friction (COF) of the samples during the scratch test at varying loads. Uniform COF was observed in the stir zone of FSPed WE43 samples compared with TMAZ and HAZ zones. Compared with the base alloy, the COF was observed as gradually decreasing from 0.35 (SZ) to 0.3 (Base region). More variations within the COF values can be observed for the base alloy around an average value of 0.35.

Fig. 12 presents the comparison of the traction forces obtained for the samples during the scratch test. The traction force (N) was observed with more variations within the measured values in the base alloy (Fig. 12(a)) compared with the FSPed WE43 (Fig. 12(b)). The average traction forces were measured as 8, 12 and 16 N for base alloy at 30, 40 and 50 N load respectively. Similarly, for FSPed alloy, the measured traction forces were observed as 10, 14, and 18 N at 30, 40 and 50 N load respectively. It can be understood that the significant microstructural changes introduced in WE43 alloy by FSP have increased the scratch resistance and hence, higher traction forces were recorded at all the loads compared with the base alloy.

Fig. 13 shows the comparison of scratch hardness in the SZ, TMAZ, and HAZ with the base alloy. The resistance offered by the material when subjected to scratch made by a sharp indenter is

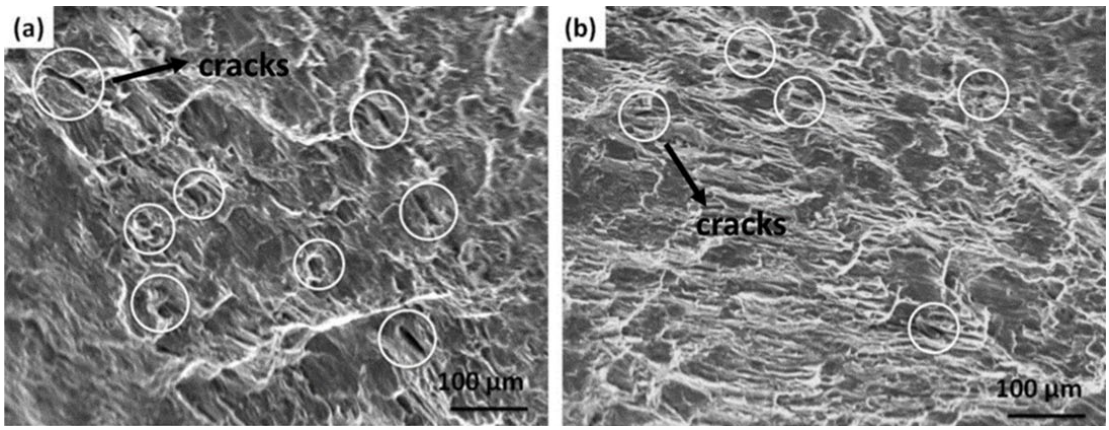

Fig. 9. Fractographs of the tensile samples obtained by SEM: (a) WE43 and (b) FSPed WE43 (c) magnified image of WE43 and (d) magnified image of FSPed WE43

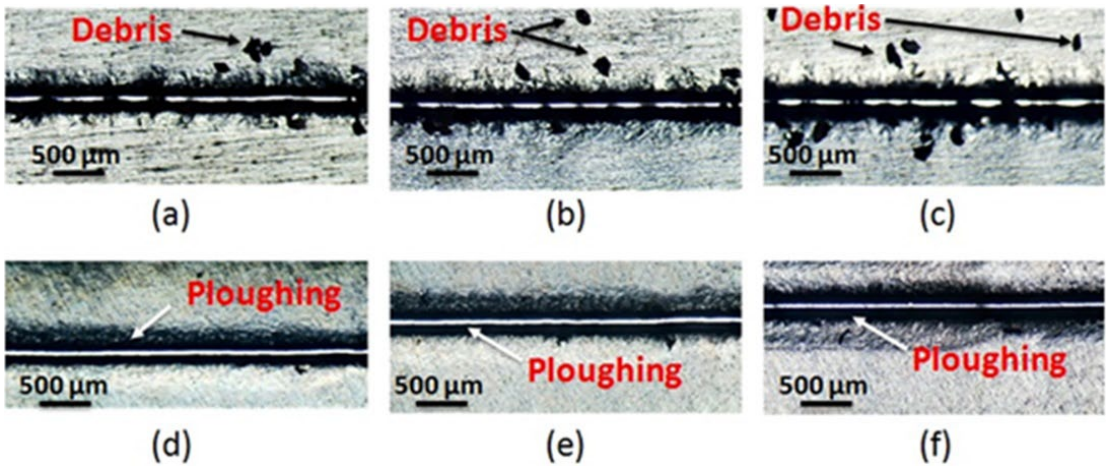

Fig. 10. Images of the scratches on the samples obtained at different loads: (a) WE43 at 30 N, (b) WE43 at 40 N, (c) WE43 at 50 N, (d) FSPed WE43 at 30 N, (e) FSPed WE43 at 40 N, (f) FSPed WE43 at 50 N

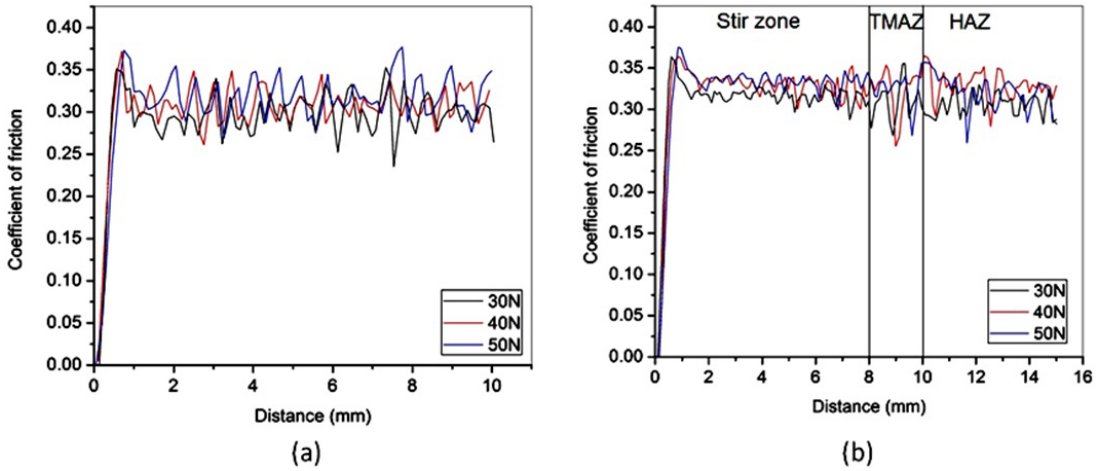

Fig. 11. Coefficient of friction of the samples at three different loading conditions during the scratch test: (a) WE43 and (b) FSPed WE43

known as scratch hardness. The wear characteristics of a surface can be assessed by the scratch test. The scratch hardness of the FSPed sample was higher compared to the base at all three loads 30 N, 40 N, and 50 N. The scratch widths for FSPed material were smaller as compared to the base alloy. The scratch with the smaller width implies a larger scratch hardness. The scratch hardness of the FSPed alloy showed a decreasing trend with respect to increasing load at all zones SZ, TMAZ and HAZ zones.

In supersaturated alloys, precipitation of intermetallics is a common observation which influence the material bulk performance. In the current work, investigations were carried out immediately after preparing the FSPed sample. Hence, the role of

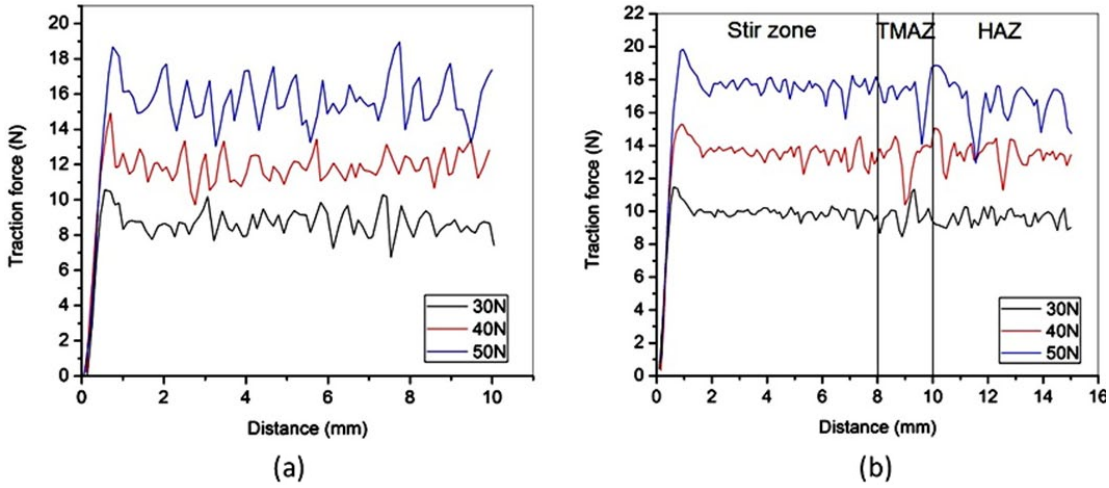

Fig. 12. Traction force at different applied loads during the scratch test: (a) WE43 and (b) FSPed WE43

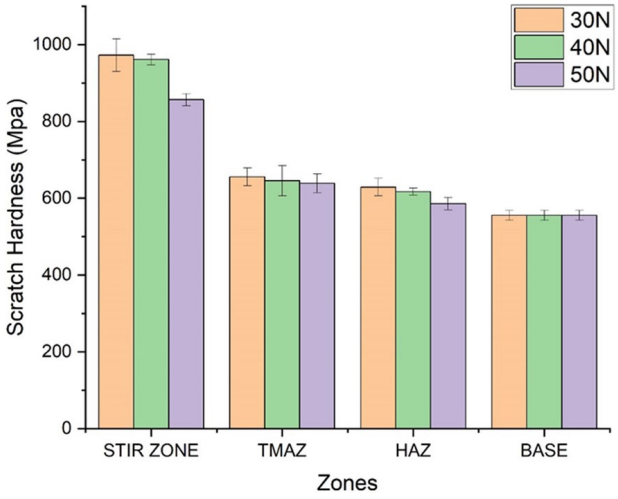

Fig. 13. Comparison of the scratch hardness of the test samples at different loads and zones

precipitated phases on the properties can be considered as negligible. However, with the aging, precipitation can be accelerated in the FSPed WE43 Mg alloy and the post-aged microstructure influence on the material properties is expected to be significant which is the scope for the future work. From the overall results, it can be summarized that FSP can be used to reduce the grain size of WE43 Mg alloy and the cumulative effect of decreased grain size, formation of super saturated grains and development of crystal texture enhance the mechanical performance. The tensile strength can be significantly improved without sacrificing much ductility, which helps to develop structures with higher load bearing capacity. Furthermore, improved scratch resistance after FSP is also favourable for developing surfaces with better tribological behaviour.

5. Conclusions

In the present work, WE43 Mg alloy was successfully processed by FSP with an aim to understand the role of altered microstructure on the mechanical and tribological properties. From the results, the following conclusions can be made.

i. It was observed that FSP led to grain refinement from 46 ± 4.2 μm to 16.1 ± 5.4 μm and also decreased the fraction of intermetallics that usually appeared in the base alloy.
ii. XRD analysis also confirms the decreased intermetallic fraction in addition to the appearance of texture after FSP.
iii. Due to the combined effect of smaller grain size, reduce intermetallics the development of supersaturated grains; the development of preferred texture; increased hardness (up to 45%) and higher tensile strength (~30%) and decreased % of elongation (~8%) have been observed. At the sacrifice of merely a smaller fraction of ductility, significant improvement in the tensile strength has been achieved.
iv. Scratch test data revealed that the FSPed alloy demonstrates better scratch resistance as appeared in the higher scratch hardness.

Hence, it is concluded that FSP can be adopted to improve the WE43 Mg alloy mechanical performance and tribological behavior by promoting grain refinement targeted for load-bearing lightweight structural applications.

REFERENCES

[1] Y. Yang, X. Xiong, J. Chen, X. Peng, D. Chen, F. Pan, Research advances in magnesium and magnesium alloys worldwide in 2020. J. Magnes. Alloy. **9** (3), 705-747 (2021). DOI: https://doi.org/10.1016/j.jma.2023.07.01

[2] M. Gupta, N. Gupta, The promise of magnesium based materials in aerospace sector. Int. J. Aeronautics. Aerospace. Res. **4** (1), 141-149 (2017). DOI: http://dx.doi.org/10.19070/2470-4415-1700017

[3] K.U. Kainer, B.L. Mordike, [ed.] Magnesium alloys and their applications, Weinheim 2000.

[4] B. Vandana, P. Syamala, D. Sri Venugopal, S.K. Imran, B. Venkateswarlu, M. Jagannatham, M. Kolenčík, I. Ramakanth, R. Dumpala, B. Ratna Sunil, Magnesium/fish bone derived hy-

droxyapatite composites by friction stir processing: studies on mechanical ehaviour and corrosion resistance, Bull. Mater. Sci, **42**, 1-10 (2019).
DOI: https://doi.org/10.1007/s12034-019-1799-z

[5] V. Badisha, S.K.R, R.S Buradagunta, Magnesium based alloys and composites: Revolutionized biodegradable temporary implants and strategies to enhance their performance. Materialia **27**, 101680 (2023).
DOI: https://doi.org/10.1016/j.mtla.2023.101680

[6] R. Davis, A. Singh, K. Debnath, P. Soares, S.H. Och, A.K. Keshri, L. Sopchenski, H.A. Terryn, Enhanced abrasive-mixed-μ-EDM performance towards improved surface characteristics of biodegradable Mg AZ31B alloy. Int. J. Adv. Manuf. Technol. **124** (7-8), 2685-2700 (2023).
DOI: https://doi.org/10.1007/s00170-022-10673-7

[7] R. Davis, A. Singh, K. Debnath, M.J. Jackson, P. Soares, F.L. Amorim, H. Dutta, Effect of Powder Particle Concentration and Tool Electrode Material amid Zinc Powder-Mixed μEDM of Biocompatible Mg Alloy AZ91D. J. Mater. Eng. Perform. **30**, 5704-5718 (2021).
DOI: https://doi.org/10.1007/s11665-021-05788-z

[8] M. Kasaeian-Naeini, M. Sedighi, R. Hashemi, Severe plastic deformation (SPD) of biodegradable magnesium alloys and composites: A review of developments and prospects. J. Magnes. Alloy. **10** (4), 938-955 (2022).
DOI: https://doi.org/10.1016/j.jma.2021.11.006

[9] B. Ratna Sunil, A. Thirugnanam, U. Chakkingal, T.S. Sampath Kumar, Nano and ultra fine grained metallic biomaterials by severe plastic deformation techniques. Mater. Technol. **31** (13), 743-755 (2016).
DOI: https://doi.org/10.1080/10667857.2016.1249133

[10] R.S Mishra, P.S. De, N. Kumar, Friction stir processing. Friction stir welding and processing: sci. eng. 259-296 (2014).
DOI: https://doi.org/10.1007/978-3-319-07043-8_9

[11] S.C Kundurti, A. Sharma, P. Tambe, A. Kumar, Fabrication of surface metal matrix composites for structural applications using friction stir processing – A review. Mater. Today. Proc. **56**, 1468-1477 (2022). DOI: https://doi.org/10.1016/j.matpr.2021.12.337

[12] W. Wang, P. Han, P. Peng, T. Zhang, Q. Liu, S.N Yuan, L.Y. Huang, H.L. Yu, K. Qiao, K.S. Wang. Friction stir processing of magnesium alloys: a review. Acta. Metall. Sin-ENGL. **33**, 43-57 (2020).
DOI: https://doi.org/10.1007/s40195-019-00971-7

[13] R.S. Buradagunta, T.S.S. Kumar, C. Uday, Bioactive grain refined magnesium by friction stir processing. In Mater. Sci. Forum. **710**, 264-269 (2012).
DOI: https://doi.org/10.4028/www.scientific.net/MSF.710.264

[14] N. Saikrishna, G.P. Reddy, B. Munirathinam, R.S. Buradagunta, Influence of bimodal grain size distribution on the corrosion behavior of friction stir processed biodegradable AZ31 magnesium alloy. J. Magnes. Alloy. **4** (1), 68-76 (2016).
DOI: https://doi.org/10.1016/j.jma.2015.12.004

[15] X. Luo, G. Cao, W. Zhang, C. Qiu, D. Zhang, Ductility improvement of an AZ61 magnesium alloy through two-pass submerged friction stir processing. Materials **10** (3), 253 (2017).
DOI: https://doi.org/10.3390/ma10030253

[16] H. Patle, R. Dumpala, R.S. Buradagunta, Machining characteristics and corrosion behavior of grain refined AZ91 mg alloy produced by friction stir processing: role of tool pin profile. Trans. Indian Inst. Met. **71**, 951-959 (2018).
DOI: https://doi.org/10.1007/s12666-017-1250-3

[17] Y. Takayama, I. Takeda, T. Shibayanagi, H. Kato, K. Funami. Superplasticity in friction stir processed AZ80 magnesium alloy. In Key Eng. Mater. **433**, 241-246 (2010).
DOI: https://doi.org/10.4028/www.scientific.net/KEM

[18] M. Venkataiah, T. Anup Kumar, K.V. Rao, S.A. Kumar, S. Irullappasamy, B. Ratna Sunil, Effect of grain refinement on corrosion rate, mechanical and machining behavior of friction stir processed ZE41 Mg alloy. Trans. Indian Inst. Met. **72**, 123-132 (2019).
DOI: https://doi.org/10.1007/s12666-018-1467-9

[19] Q. Yang, A.H. Feng, B.L. Xiao, Z.Y. Ma, Influence of texture on superplastic behavior of friction stir processed ZK60 magnesium alloy. Mater. Sci. Eng. A. **556**, 671-677 (2012).
DOI: https://doi.org/10.1016/j.msea.2012.07.046

[20] V. Jain, R.S. Mishra, R. Verma, E. Essadiqi, Superplasticity and microstructural stability in a Mg alloy processed by hot rolling and friction stir processing. Scr. Mater. **68** (7), 447-450 (2013).
DOI: https://doi.org/10.1016/j.scriptamat.2012.11.009

[21] Q. Yang, B.L. Xiao, Q. Zhang, M.Y. Zheng, Z.Y. Ma, Exceptional high-strain-rate superplasticity in Mg–Gd–Y–Zn–Zr alloy with long-period stacking ordered phase. Scr. Mater. **69** (11-12), 801-804 (2013).

[22] X. Xu, X. Chen, W. Du, Y. Geng, F. Pan, Effect of Nd on microstructure and mechanical properties of as-extruded Mg-Y-Zr-Nd alloy. J. Mater. Sci. Technol. **33** (9), 926-934 (2017).
DOI: https://doi.org/10.1016/j.jmst.2017.04.011

[23] M. Yamasaki, K. Hashimoto, K. Hagihara, Y. Kawamura, Effect of multimodal microstructure evolution on mechanical properties of Mg–Zn–Y extruded alloy. Acta Mater. **59** (9), 3646-3658 (2011).
DOI: https://doi.org/10.1016/j.actamat.2011.02.038

[24] B.N. Du, Z.Y. Hu, L.Y. Sheng, D.K. Xu, Y.X. Qiao, B.J. B.J. Wang, J. Wang, Y.F. Zheng, T.F. Xi, Microstructural characteristics and mechanical properties of the hot extruded Mg-Zn-Y-Nd alloys. J. Mater. Sci. Technol. **60**, 44-55 (2021).
DOI: https://doi.org/10.1016/j.jmst.2020.05.021

[25] J. Li, D.T. Zhang, F. Chai, W. Zhang, Microstructures and mechanical properties of WE43 magnesium alloy prepared by friction stir processing. Rare. Met. **39**, 1267-1272 (2020).
DOI: https://doi.org/10.1007/s12598-014-0306-3

[26] A.R. Eivani, M. Mehdizade, S. Chabok, J. Zhou, Applying multi-pass friction stir processing to refine the microstructure and enhance the strength, ductility and corrosion resistance of WE43 magnesium alloy. J. Mater. Res. Technol. **12**, 1946-1957 (2021).
DOI: https://doi.org/10.1016/j.jmrt.2021.03.021.

[27] L. Kunčická, P. Král, J. Dvořák, R. Kocich, Texture Evolution in Biocompatible Mg-Y-Re Alloy After Friction Stir Processing. Metals **9**, 1181 (2019).
DOI: https://doi.org/10.3390/met9111181

[28] B. Wu, F. Yusof, F. Li, B.B.A. Razak, M.R.B. Muhamad, I.A. Badruddin, M. Hussien, S. Kamangar, M.Z. Ibrahim, Influence of Friction Stir Processing Parameters on Microstructure,

Hardness and Corrosion Resistance of Biocompatible Mg Alloy WE43. Arab. J. Sci. Eng. **49**, 1897-1911 (2024).
DOI: https://doi.org/10.1007/s13369-023-08037-8

[29] B. Ratna Sunil, Surface Engineering by Friction Assisted Processes, CRC Press, Taylor & Francis, New York, USA (2019).

[30] G.V.V. Surya Kiran, K. Hari Krishna, S.K. Sameer, M. Bhargavi, B. Santosh Kumar, G.M. Rao, Y. Naidubabu, R. Dumpala, R.S Buradagunta, Machining characteristics of fine grained AZ91 Mg alloy produced by friction stir processing, T. Nonferr. Metal. Soc. **27** (4), 804-811 (2017).
DOI: https://doi.org/10.1016/S1003-6326(17)60092-X

[31] J. Li, D.T. Zhang, F. Chai, W. Zhang, Microstructures and mechanical properties of WE43 magnesium alloy prepared by friction stir processing. Rare Met. **39**, 1267-1272 (2020).
DOI: https://doi.org/10.1007/s12598-014-0306-3

[32] H. Seifiyan, M. H. Sohi, M. Ansari, D. Ahmadkhaniha, M. Saremi, Influence of friction stir processing conditions on corrosion behavior of AZ31B magnesium alloy. J. Magnes. Alloys **7** (4), 605-616 (2019). DOI: https://doi.org/10.1016/j.jma.2019.11.004

[33] K.J. Sandeep, A.K. Choudhary, R.J. Immanuel, Microstructural Characterization and Mechanical Performance of AZ91 Magnesium Alloy Processed by Friction Stir Processing Using Novel Tool Designs. J. Mater. Eng. Perform. **33**, 120-135 (2024).
DOI: https://doi.org/10.1007/s11665-023-07980-9

[34] H.-X. Cao, X.-Y. Wu, H.-M. Liao, M.-Y. Hao, Development of Processing Maps for AZ81E Magnesium Alloy. High Temp. Mater. Proc. **37** (2), 157-162 (2018).
DOI: https://doi.org/10.1515/htmp-2016-0082

[35] P.K.A. Babu, U.S. Karle, Y. Ambhore, Ch. Chowdary, Role of temperature and strain rate on evolution of microstructure, flow stress and constitutive equation in hot deformation of AZ80A Mg alloy. Int. J. Mater. Form. **15**, 76 (2022).
DOI: https://doi.org/10.1007/s12289-022-01722-3